Annex E

SENSITIVITY ANALYSIS OF THE OCEANIC TRANSPORT MODULE

In this Annex we present sensitivity studies with respect to some processes governing POP behaviour in soil and seawater environmental compartments.

The World Ocean is one of the most capacious medium for some persistent organic pollutants. POPs enter the seawater mainly from the atmosphere by depositions and gaseous exchange as well as with river run-offs. Concentration field variations in the World Ocean take place due to seawater horizontal and vertical currents, POP partitioning between the dissolved phase and phases sorbed of different suspended particles and dissolved organic compounds, deposition of sorbed phases together with sedimentating particles, resuspention processes in the near bottom layers, degradation and a number of other processes. With the availability of ice coverage on the sea surface, POPs from the atmosphere are accumulated on the ice surface and drift with ice over large distances then with melting water enter the marine environment.

The current version of the hemispheric model includes the following processes describing the behaviour of a pollutant in the marine environment

- horizontal currents and vertical motion of water masses,
- distribution over the upper mixing layer, which changes dynamically,
- three-dimensional turbulent diffusion,
- POP partitioning between the dissolved phase and phases adsorbed on suspended particles,
- POP sedimentation with particles,
- influence of ice cover on POP transport,
- POP degradation.

In the current version of the model influence of ice cover, sedimentation and partitioning between different POP phases in seawater are described in quite a rough way. However, they can inflict an appreciable impact on some POPs budget ratios in the seawater. Below we present the investigation of model sensitivity to POP partitioning between different phases and processes connected with sea ice environment (simplified version). In this section we evaluate model sensitivity with respect to processes of POP partitioning in the marine environment and to consideration of ice cover.

E.1. POP partitioning between different phases

Model assumptions. POP redistribution between the dissolved phase and the phase associated with particles essentially affects the dynamics of POP concentration fields in the marine environment. Under the condition of instantaneous phase equilibrium establishment the relation between particulate and dissolved phases is as follows:

$$c_p = k^p \cdot c_d \,. \tag{E.1}$$

In its turn k^p may be estimated by the expression:

$$k^p = k_p^o K_p c_{prt} \qquad \text{(E.2)}$$

where k_p^o is fraction of organic matter in a particle;

K_p is equilibrium constant for sorption/desorption processes (proportional to octanol-water coefficient K_{OW});

C_{prt} is particle concentration.

The concentration of sedimentating particles in the seawater to a considerable extent is defined by the availability of phytoplankton organisms evolving in the upper layers [*Tusseau et al.,* 1997]. Phytoplankton being a primary producer of carbon compounds in the seawater gives rise to the evolution of subsequent organisms in the food chain. As a result of biosystem evolution in the upper layer a flux of organic carbon in a particle form makes its way to the bottom. For the phytoplankton evolution a sufficient quantity of light energy and inorganic nutrient are required. The intensity of light energy in the upper layers (euphotic zone) depends on a season. The availability of inorganic nutrient depends on different characteristics of the marine environment: temperature, current pattern, vertical mixing, closeness of riverine and coastal runoff etc. The global pattern of phytoplankton intensity distribution is extremely complex and dynamic. In the majority of sea basins annual variation of phytoplankton evolution is characterized by the growth peak in spring ("spring blossom") and subsequent minimum intensity in summer [*Dale et al.,* 1999; *Dutkiewicz et al.,* 2001; *Jackson and Burd,* 2002]. As a very rough approximation we presume that the annual cycle of phytoplankton evolution intensity and correspondingly organic particle concentrations is like the curve depicted in Figure E.1.

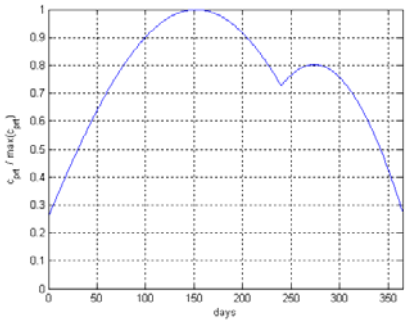

Figure E.1. *Dependence of particle concentrations in an annual cycle for middle latitudes*

Temperature conditions, the pattern of horizontal and vertical currents and internal properties of the evolution of marine ecocommunities is defined by the availability of productive (eutrophic) and underproductive (oligotrophic) zones [*Monin,* 1997; *Garcon et al.,* 2001]. The distribution of mean annual productivity over the World Ocean is demonstrated in Figure E.2.

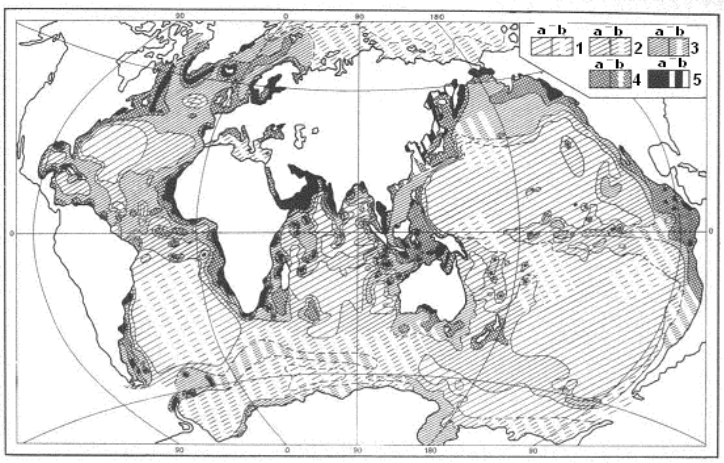

Figure E.2. *Mean annual productivity distribution (mg/m^2) over the World Ocean* [*Monin,* 1997]
1– <100, 2 – 100-150, 3 – 150-250, 4 – 250-500, 5 – >500
***a** – by radionuclide method, **b** – by indirect methods*

In a first approximation at zonal averaging it may be supposed that waters in middle latitudes are most productive therefore the dependence of particle concentrations in the seawater on latitude shown in Figure E.3 is used.

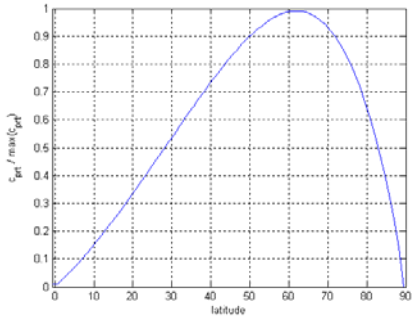

Figure E.3. *Dependence of particle concentrations in the ocean on latitude*

The sedimentation process of organic particles is characterized by particle concentration decline with depth due to the formation of dissolved organic compounds and particle size increase as a result of coagulation. For this reason in the model the dependence of particle concentration on depth looks as displayed in Figure E.4 and particle sedimentation velocity – like in Figure E.5.

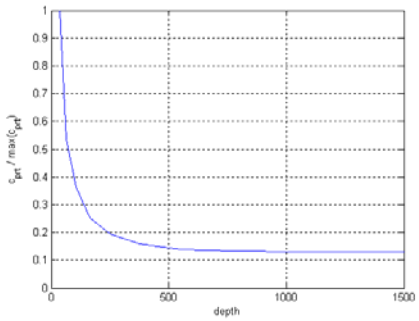

Figure E.4. *Dependence of particle concentrations on the seawater depth*

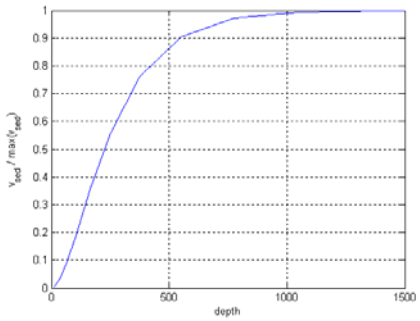

Figure E.5. *Dependence of particle sedimentation velocity on the depth*

Numerical experiments. To examine the developed model efficiency numerical experiments for the assessment of PCB transport over the Northern Hemisphere have been carried out. POP dynamics module for the seawater was integrated to the hemispheric multi-compartment model MSCE-POP. PCB emission scenario was prescribed on the base of available data for Russia [*AMAP Repot 2000:3,* 2000] and for Europe [*Pacyna et al.,* 1999].

POP transport dynamics in sea was calculated with the time step of 1 hour in knots of the calculation grid with horizontal spatial resolution 1.25^0x1.25^0 and vertical layer depths 12.5, 37.5, 65.0, 105.0, 250.0, 375, 550, 775, 1050, 1400, 1900, 2600, 3500, 4600 meters. Values of the velocity fields and the upper mixing layer thickness for sea were updated every day from previously prescribed data file [*Zelenko and Resniansky,* 1999] and it was interpolated for each time step. In the preliminary ("basic") experiment the model spin-up was performed, that is calculations for a year period were repeated with input parameters of the same year. Characteristic of the marine environment affecting equilibrium constants between the dissolved and sorbed phase (particle concentration, organic matter content in particles, equilibrium coefficient K_{OW}) and particle sedimentation velocities (particle density and size) were selected in such a way that the dissolved phase concentration was equal to that of the sorbed one [*Schulz-Bull et al.,* 1998] and particle sedimentation velocity – about 100 m/day [*Baldwin et al.,* 1998]. In the basic experiment sedimentation velocity did not depend on time and spatial co-ordinates. For the calculated period of about 30 years the model system has achieved quasi-steady state (like annual variation of dynamic fields). Figures E.6-E.8 show plots for PCB mass mean annual variation in the environmental compartments.

From the comparison of PCB mass dynamics in different environmental compartments (Fig. E.8) it is possible to conclude that most inertial is soil (Fig. E.6). PCB distribution over the seawater at the selected parameters is established during approximately 10 years (Fig. E.7). In subsequent experiments it was shown that at the decrease of sedimentation velocity by two orders of magnitude or similar reduction of the coefficient of phase partitioning (shift of distribution to the dissolved phase) the period of process establishment in the seawater was similar to that in soil (about 30 years). Figure D.17 demonstrates the dynamics of PCB mass loss velocities (outflow through the atmospheric boundaries, sea current transport through the equator, sedimentation to the seawater, pollutant degradation) for different environmental compartments. It is evident that about one third of PCB mass entering the environment is lost via seawater.

Figure E.6. *PCB mass dynamics in soil*

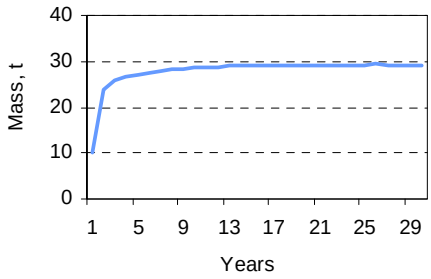

Figure E.7. *PCB mass dynamics in the seawater*

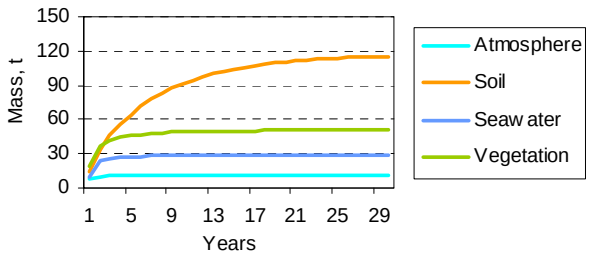

Figure E.8. *PCB mass dynamics in different compartments*

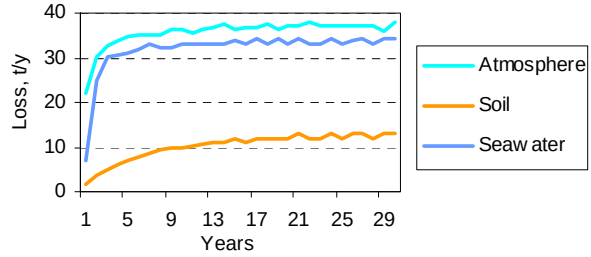

Figure E.9. *Dynamics of PCB mass loss velocity in different compartments*

In the experiment the highest concentrations were observed in internal seas and coastal zones. This distribution may be explained first by emission source distribution (Europe, Russia) and second by the absence of transport and sedimentation mechanisms in internal seas and coastal zones (cells with non-zero content of land elements) in the basic experiment.

In view of importance of sedimentation processes for the problem of POP distribution in the environment experiments with refined parameter influencing the sedimentation velocity. These parameters are the phase partitioning coefficient (in its turn depending upon particle concentrations) and the particle sedimentation velocity.

To evaluate the effect of heterogeneity and no steady state of phase partitioning coefficient we conducted experiments aimed at studying the dependence of particle concentrations on time, latitude and depth (Figs. E.1, E.3, E.4) of the integral dependence (the product of dependence on time, latitude and depth). Alongside the dependence of phase partitioning coefficient on depth, the dependence of particle sedimentation velocity shown in Figure E.5 was also introduced. All dependences of particle concentrations employed the normalization condition:

$$\frac{1}{T}\int_0^T (\frac{1}{V}\int_V k(\lambda,\varphi,z,t)dv)dt = \frac{1}{T}\int_0^T (\frac{1}{V}\int_V k^p dv)dt = 1, \qquad \text{(E.3)}$$

where T is annual period;
V is volume of the calculated water reservoir.

As follows from Figures E.10 and E.11, introduction of particle concentration dependence on time, latitude and depth insignificantly changes integral characteristics of the system. At the combined dependence PCB mean annual mass in the seawater declines and PCB mass loss velocity for seawater increases.

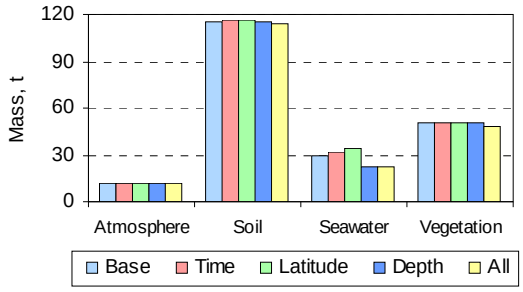

Figure E.10. *PCB mean annual masses in different compartments in the basic experiment and in the experiment with phase partitioning coefficient dependence on time, latitude and depth and integral dependence*

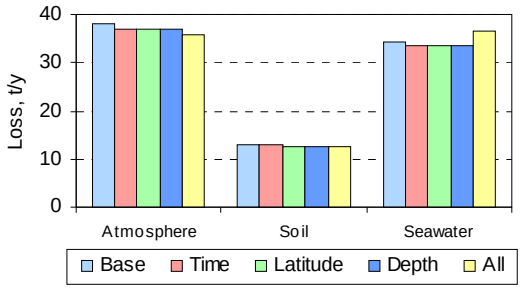

Figure E.11. *PCB annual mass loss velocity in different compartments in the basic experiment and in the experiment with phase partitioning coefficient dependence on time, latitude and depth and integral dependence*

Changes in the redistribution of concentration fields in the sea reservoir (Fig. E.12 compared to Fig. E.13) are more pronounced. In this experiment PCB concentration increases in regions of the open seawater manifesting the effect of sea currents on concentration field distributions.

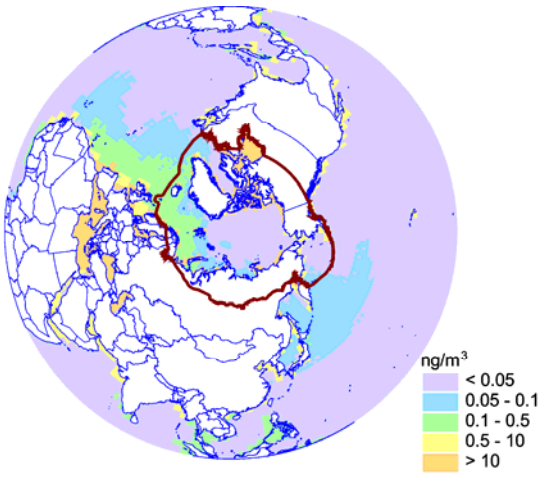

Figure E.12. *PCB mean annual total concentration in the upper seawater layer in the basic experiment*

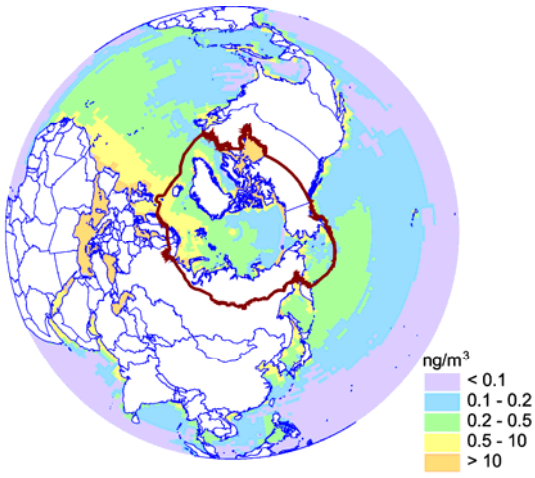

Figure E.13. *PCB mean annual concentration in the upper seawater layer for combined dependence of phase partitioning dependence on time, latitude and depth*

For further clarification of the effect of phase partitioning coefficient and particle sedimentation were performed experiments with maximum particle concentration max(c_{prt}) in dependences given in Figures E.1, E.3 and E.4 the integral coefficient of phase partitioning k^p from (E.1) decreases 10 times (experiment “Dissociation/10) and 100 times (experiment “Dissociation/100”).

In a similar manner due to the uncertainty in mean diameter d^p and particle density ρ_o^p resulting in scattering of $max(v_{sed})$ (Fig. E.5) experiments with $max(v_{sed})$ reduced as much as 10 times “Sedimentation/10”) and 100 times (“Sedimentation/100”) were performed. Diagrams of experimental results are demonstrated in Figures E.14–E.16.

As seen from Figures E.14 and E.15, PCB mass variation in the seawater is mostly affected by the phase partitioning coefficient and the rate of PCB removal outside the seawater calculation domain – by the particle sedimentation velocity. The variation of phase partitioning coefficient essentially affects PCB flux from the atmosphere to the seawater (Fig. E.16).

As follows from the comparison of Figures E.13 and E.17 decrease of sedimentation velocity by 2 orders increases PCB concentration in the upper layer by an order of magnitude and more.

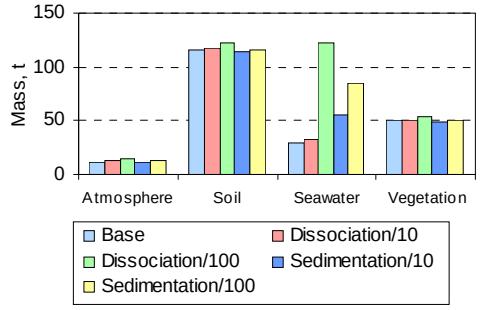

Figure E.14. *PCB mean annual mass in different environmental compartments in the basic experiment and in experiments with reduced phase partitioning coefficient and particle sedimentation velocity*

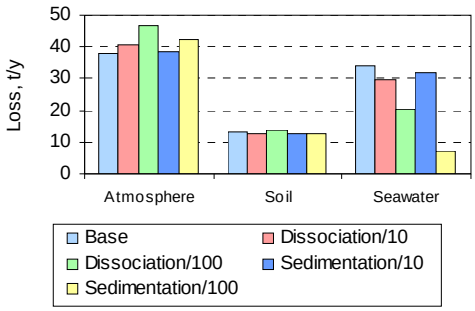

Figure E.15. *PCB annual mass loss velocity in different environmental compartments in the basic experiment and in experiments with reduced phase partitioning coefficient and particle sedimentation velocity*

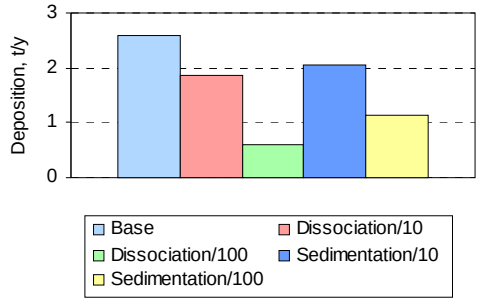

Figure E.16. *PCB annual fluxes from the atmosphere to the seawater in the basic experiment and in experiments with reduced phase partitioning coefficient and particle sedimentation velocity*

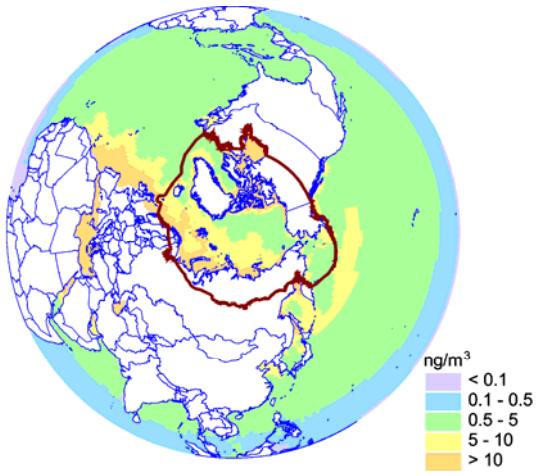

Figure E.17. *PCB total mean annual concentration in the upper seawater layer for particle sedimentation velocity decreased 100 times in comparison with the velocity in the basic experiment*

E.2. POP transport with ice cover

In the hemispheric version of the model for proper description of the processes consideration of the ice cover is highly desirable. In the review [*Macdonald et al.,* 2000], it was pointed out, that sea ice has a potentially important role in the transport of contaminants. In particular, much of the ice in the Arctic is produced in shallow marginal seas during winter and exported to the interior seawater. Ice forming on shelves can incorporate contaminated sediments during suspension freezing, frazil ice formation or from bottom-anchored ice. This contaminated ice may then be transported thousands of kilometers undergoing little or no alteration. Besides, the ice cover acts as a barrier to exchange of gases including POP vapor-phase, limiting their direct entry from the atmosphere and evasion from sea to air.

Model assumptions. The ice module of POP transport describes the following processes:

- accumulation in the snow thickness and on the ice surface,
- gas phase exchange between the snow and the atmosphere,
- fluxes into the seawater as a result of snow and ice melting,
- fluxes from the seawater to the ice cover during ice bottom and lateral accretion,
- horizontal transport with drifting ice,
- degradation in the snow and ice environment.

Sea ice plays the role of a screen between the seawater and the atmosphere. At the same time POP may be accumulated in ice itself and in the snow above it. On the upper snow-ice surface the process of POP exchange with the atmosphere takes place. When snow and ice are melting on the surface and melting or frosting on the lower or lateral surfaces, POP pass to the water environment and return back. Besides POP trapped by the sea ice and snow thickness may be transported with ice drift.

Modules of POP dynamics in the marine ice cover were switched to the MSC-E multi-compartment model of POP transport. For the ice module the horizontal grid and time step were: horizontal step 1.25^{o} x 1.25^{o}, time step – 1 hour. Fields of snow and ice thickness, ice and snow melting rate, snow-ice surface temperature, ice drift velocity were read on the monthly basis from files previously calculated and were interpolated for each time step (see Section E.5 below).

Numerical experiments. The sensitivity of global POP transport model to the developed sea ice model was tested by numerical experiments of the global dispersion of selected POP (PCB-153) within the Northern Hemisphere.

Below we describe the results of the following numerical experiments.

- In the “Base” experiment PCB-153 concentrations were calculated for the period from 1970 to 1996. In this experiment we used the model of POP flux through the sea ice cover with additional introduced vertical “mixing” of POP concentrations in the snow and ice environment roughly parameterizing POP fluxes due to mechanical (hummocking) and thermal (melting) processes.
- The experiment “Noice 1994” was similar to the “Base” experiment, in which from 1994 to 1996 the sea ice cover was neglected. As initial concentration fields here appropriate fields for late 1993 from the “Base” experiment were selected.
- “Noice 1970” with parameters like in the “Base” but in this case sea ice cover was not considered from the beginning of the experiment (from 1970). POP initial concentrations equaled zero.

- "Nomix" was similar to the "Base" but in this experiment POP concentration "mixing" in the snow and ice environment was not calculated from 1994 to 1996. POP initial concentrations were the same as in the "Base" for late 1993.
- "Nodyn" with parameters as in the "Base" but without drift of the sea ice cover. The initial concentrations were zero.

The experiments "Noice 1994" and "Noice 1970" were aimed at studying the extent of sea ice cover impact on the dynamics of POP environmental concentrations. The "Nomix" results allow us to assess the effect on the introduced vertical mixing of POP concentrations between snow and ice. The experiment "Nodyn" was carried out for the evaluation of contribution of sea ice drift to the processes studied.

The comparison results of PCB-153 concentrations measured in seawater of different basins during the considered period with concentrations calculated in the experiment is shown in Table E.1.

The column "Calculated values" shows the lowest and the highest mean monthly values of PCB-153 concentrations for the reference year. The comparison of calculated against measured values demonstrates that the parameterization of POP transport processes in the marine environment including the transport through the ice cover is adequate enough.

Table E.1. *The comparison results of PCB-153 concentrations measured in seawater with concentrations in the experiment "Base" (ng/m^3)*

Year	Region	Geographical co-ordinates	Measured values	Calculated values	Reference for measured data
1986	North Atlantic	47-48N, 20-21W	0.34 – 2.70	1.07 – 1.63	*Broman and Axelman*, 1997
1986	Ice Island	81N, 97W	0.56	0.55 – 0.93	
1988	North Sea	54N,1.6E	4.77	17.1 – 32.82	*Schulz-Bull et al*., 1991
1989	North Atlantic	40N, 40W	2.10	0.29 – 0.79	*Broman and Axelman*, 1997
1989	Caribbean Sea	15N, 70W	1.45	0.51 – 0.98	
1989	Gulf of Mexico	25N, 90W	1.29	0.28 – 0.4	
1989	Mediterranean Sea	35N, 20E	2.18	1.84 – 2.91	
1990	Chukchi Sea	70N,180E	0.68	0.33 – 0.59	
1990	Bering Sea	62N,170W	0.97	0.18 – 0.75	
1990	Gulf of Alaska	55N,150W	0.97	0.2 – 0.46	
1990	Pacific Ocean	40-50N,180E	1.13 – 1.14	0.14 – 0.68	
1990	New Bedford Bay	41N, 71W	1.45	0.58 – 1.3	*Bergen et al*., 1993
1992	North Atlantic	47-53N, 20-21W	0.10 – 0.40	0.52 – 1.12	*Broman and Axelman*, 1997
1993	North Atlantic	61-68N, 6-33W	0.13 – 1.21	0.14 – 0.93	*Schultz-Bull et al*., 1998
1994	Baltic Sea	54.1-57.2N, 10.6-17.5E	16.30 – 24.7	8.51 – 20.72	*Bigner et al.*, in Background document, No.64B
1995	Japanese Sea	42.8-43.4N, 139.5-140.1E	0.035 – 0.6	0.32 – 0.65	*Kannan et al*., 1998

To estimate the effect of ice cover on concentration fields in various media incorporated to the model of POP global transport, numerical experiments with no ice on the ocean surface were made. In the experiment "Noice1994" PCB-153 concentration fields were calculated on the assumption that there is no ice in the Arctic from 1994 to 1996 included.

Figures E.18 and E.19 manifest the following result: the incorporation of the ice coverage increases PCB-153 concentration in the ocean and decreases it in the atmosphere. This "behaviour" of the

model may be explained by the fact that during the considered period (1994-96) the intensity of emission sources cut down (Fig. E.20) and the ocean became an additional POP emission source. In this case the ice coverage impedes POP to pass on to the atmosphere from the ocean thereby increasing concentrations in the ocean and decreasing them in the atmosphere.

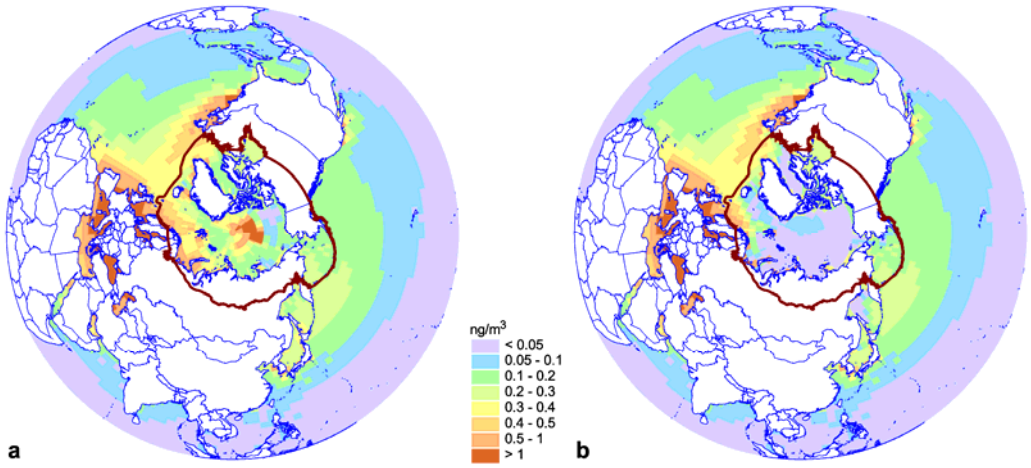

Figure E.18. *Mean annual PCB-153 concentrations in the upper ocean layer for 1996 in the "Base" experiment with ice cover (a) and the experiment "Noice1994" without ice cover (b)*

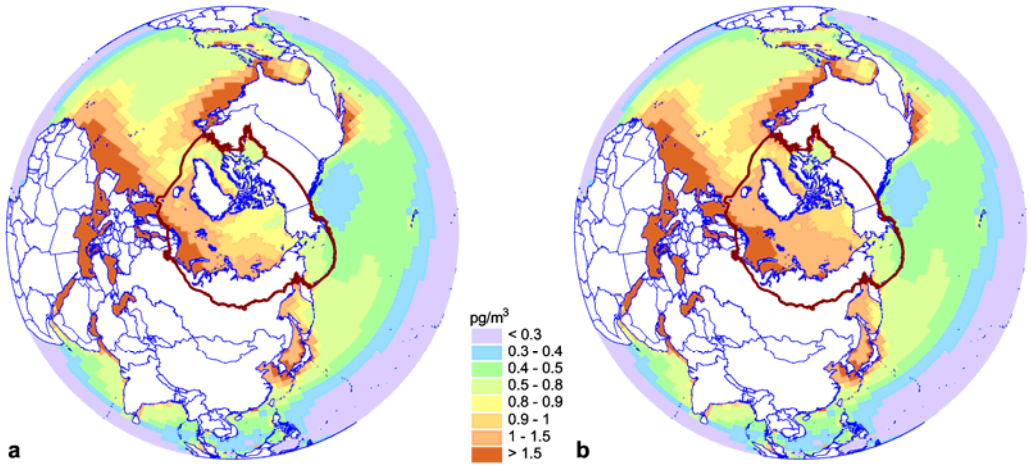

Figure E.19. *PCB-153 mean annual concentrations in the lower atmosphere for 1996 in the "Base" experiment with ice cover (a) and the experiment "Noice1994" without ice cover (b)*

Figure E.21 demonstrates the decrease of the pollutant content in the marine environment during 1994-96. This confirms the supposition about POP mass transfer from the ocean to the atmosphere during this period.

In the experiment "Noice1970" the initial concentration was assumed to be zero. During the increase of emission intensity, e.g. in 1972, (see Figs. E.20 and E.21) the ocean accumulates the pollutant mass coming from the atmosphere. Figures E.22 and E.23 present PCB-153 concentration fields in the ocean and in the atmosphere with the availability of the ice cover and without it.

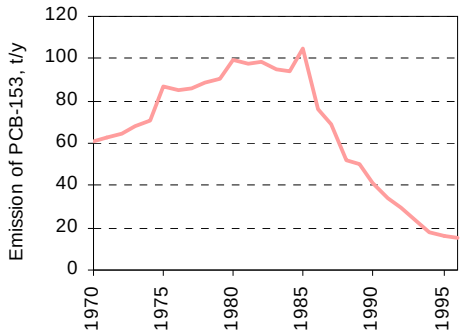

Figure E.20. *PCB-153 emissions during the calculated period*

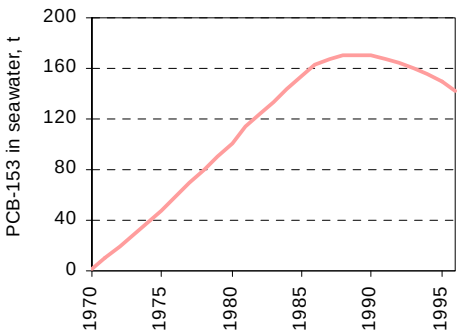

Figure E.21. *Computed PCB-153 mass in seawater during the calculated period*

The comparison of Figures E.22.a and E.22.b allows the following conclusion. Under the condition of POP intensive inflow from the atmosphere to the ocean the ice makes a screening effect.

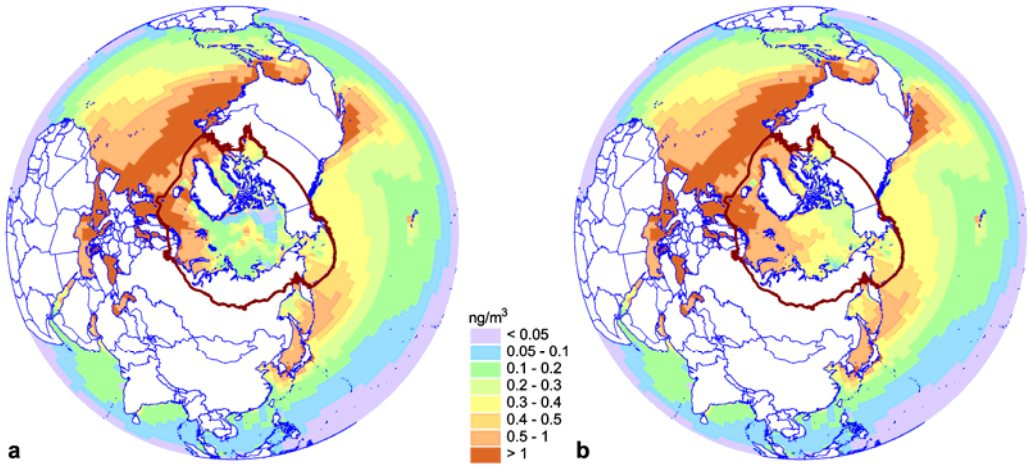

Figure E.22. *PCB-153 mean annual concentrations in the top ocean layer in the experiments "Base" (a) and "Noice1970" (b) for 1972*

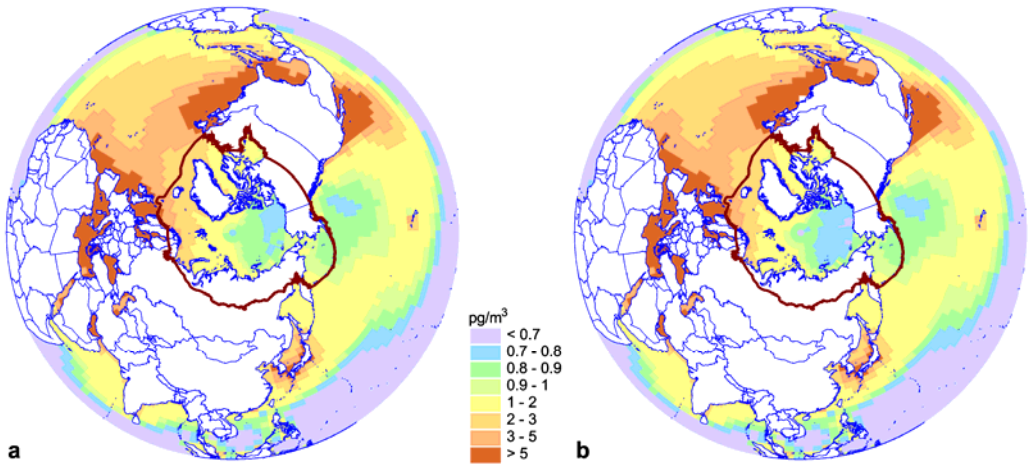

Figure E.23. *PCB-153 mean annual concentrations in the lower atmospheric layer in the experiments "Base" (a) and "Noice1970" (b)*

PCB-153 mean annual concentrations in the atmosphere in the experiment “Base” are slightly lower (D.23.a) than in the “Noice1970” without ice. This effect can be also explained by the screening effect of the ice cover.

POP mean annual concentration field in ice and snow in the experiment “Base” for 1996 is shown in Figure E.24.a. Figure E.24.b presents PCB-153 mean annual concentration field in the ice environment for the experiment “Nomix”, in which the “mixing” mechanism of POP concentrations in snow and ice is absent.

PCB-153 concentrations in ice in the experiment with concentration “mixing” in the snow and ice compartments (Fig. E.24.a) are appreciably higher than in the experiment without “mixing” (Fig. E.24.b). In the experiment “Nomix” in the absence of “mixing” in snow the concentrations reach considerable values (Fig. E.25). However, POP mass in snow is insignificant due to a small thickness of snow in the model (about 10 centimeters).

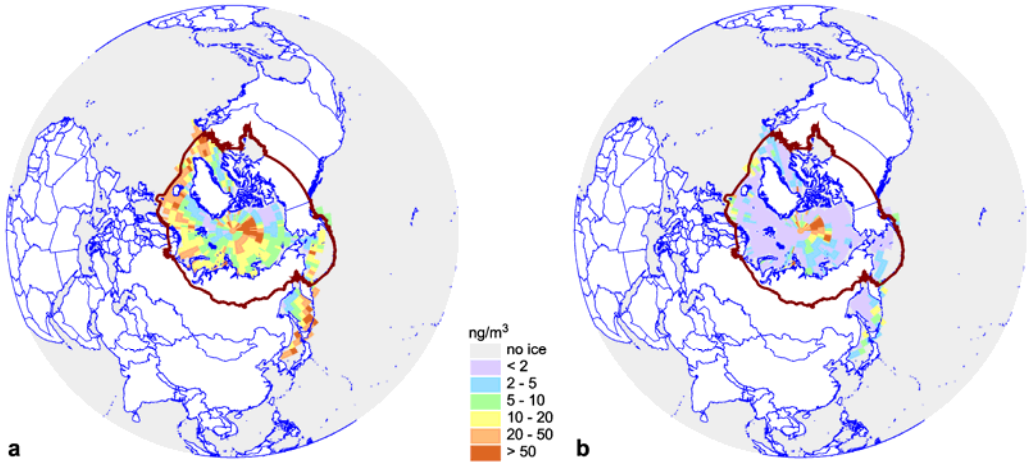

Figure E.25. *PCB-153 mean annual concentrations in 1996 in snow and ice in the experiment “Base” (a) with “mixing” of POP concentrations in the snow and ice compartments in the experiment “Nomix” (b) (without “mixing”)*

In the experiment “Base153” two extreme cases of parameterization of POP exchange between snow and ice compartments were assumed: absence of exchange and complete “mixing”. Obviously in reality some medium variant of exchange is realized: intrusion of POP molecules to the depth of snow and ice with melting water and mechanical mixing of media (humocking). According to measurement data PCB concentrations in ice in the Arctic exceed PCB concentrations in water as much as several times [*Pfirman,* 1995]. It better correlates with the experiment “Nomix”. As follows from the numerical experiments, in the formulation of the problem “mixing” in snow and ice media does not exert a considerable effect on concentrations fields in the atmosphere and ocean.

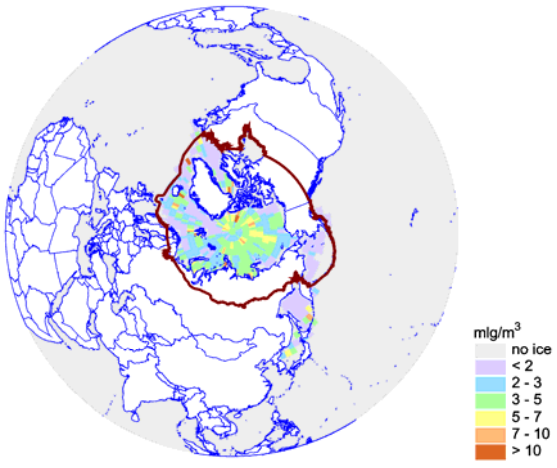

Figure E.25. *PCB-153 mean annual concentrations in 1996 in snow without “mixing” of POP concentrations in the snow and ice compartments*

A patch of elevated concentration in the experiment “Base” (Fig. E.26.a) in the region of Beaufort Sea coincides with the center of anticyclonic ice motion. The experiment “Nodyn” explains the reason for this patch. In this experiment sea ice drift was taken to be zero and no patch was observed in the Beaufort Sea (Fig. E.26.b). Results of this experiment testify that in the Beaufort Sea zones of PCB-153 accumulation are formed due to anticyclonic ice motion in this region.

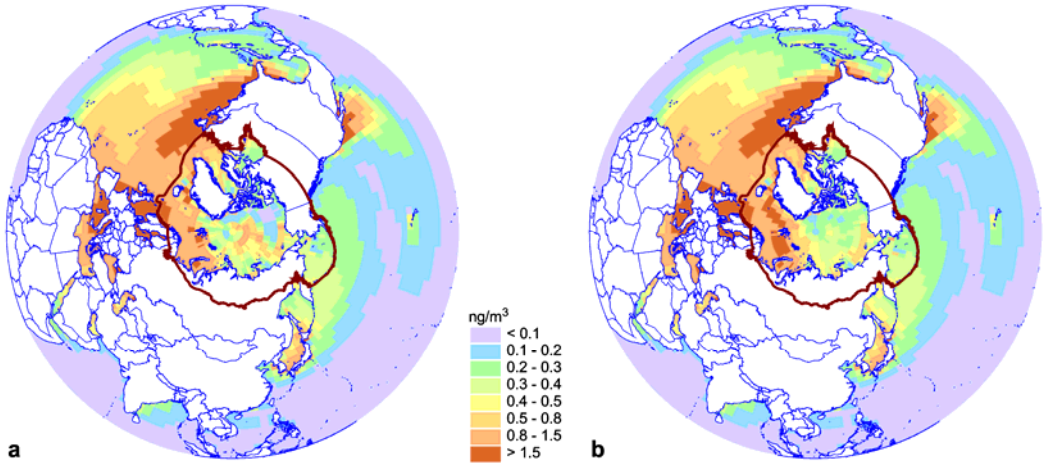

Figure E.26. *PCB-153 concentrations in August 1972 in the marine environment in the experiment “Base” (a) and “Nodyn” (b), in which sea ice drift is absent*

E.4. Model development

Further development of models of POP transport in the marine environment and sea ice cover is supposed to be performed in the following directions:

For POP marine transport model:

- Model should take into account different type of particles adsorbing POPs in seawater: bacteria cells, phytoplankton, microzooplankton, detrit, and particles with inorganic nucleum. Dissolved organic species able to sorbe POP molecules are also to be taken into account as POP carriers.
- Global 3D dynamic fields of concentrations of particles and dissolved organics in seawater are needed as model input. Such fields can be obtained on the basis of appropriate mathematical models.
- POP balance equations should take into account external POP sources such as rivers, coastal zones, etc.
- Parameterization of dynamic redistribution between sediments and seawater at ocean bottom is required.
- In parameterization of turbulent diffusion processes the dependence of diffusion coefficients on the characteristics of current velocities and other parameters of calculation domain is required.

For POP dynamics in ice/snow cover of the ocean:

- The exchange of POP containing in snow/ice environment with ocean and the atmosphere occurs mainly in surface layers. Under these conditions vertical distributions of POP concentrations in snow and ice may be essential. For more adequate description of exchange processes between

snow/ice cover, ocean and the atmosphere further parameterization of POP dynamics in the bulk of snow/ice taking into account vertical concentration profile, precipitation types (rain/snow), ice temperature, etc. is required.

- The presence of water in ice and snow leads to changes of physical parameters of ice/snow and to redistribution of all POP phases in snow/ice environment. To take this redistribution into account both description of POP redistribution dynamics and physical characteristics of snow/ice (presence of water phase, temperature, specific surface area of ice crystals, etc) is needed.

E.5. Seasonal evolution of sea ice

In this section we consider issues related to obtaining sea ice evolution characteristics for modeling the contaminants transport in the Northern Hemisphere.

The evolution of the ice cover in the Arctic is governed by a great number of interconnected physical processes going on in the atmosphere, ocean and land. The present-day monitoring system allows us to receive on a regular basis only information about very limited number of the Arctic ice state parameters. First of all these are data on ice cover compactness and its extension obtained from several satellite systems. Direct observations of other parameters are of a fragmentary character and they make it impossible to obtain regular estimates of the sea ice evolution affecting processes of contaminants transport in the Arctic. In this situation modern numerical models become basic tools for the acquisition of required quantitative information about ice cover variability.

The description of sea ice dynamics is rather a complicated problem in terms of physics and computations. The sea ice cover is very fragmentary multi-component medium consisting of variety of ice proper, snow, firn, water and sea salt. This medium is non-uniform, possesses essential anisotropy both in horizontal and vertical directions. Besides the basic component of the medium, ice, is a crystal body with a complicated behaviour at mechanical loads (rheology).

E.5.1. *Basic approaches to sea ice modeling*

Originally sea ice models were one-dimensional and accounted for main thermodynamic processes involving vertical heat redistribution along the relevant phase transfers of water in the idealized horizontally uniform ice cover.

The next step of sea ice thermodynamic model development was so-called “dynamic” models. These models additionally accounted for processes of momentum redistribution in horizontally non-uniform medium, which in fact is sea ice. These models are more sophisticated since they describe mechanical interactions in the fragmentary ice cover with varying compactness within the framework of sea ice cover as a continuous media. Presumably the first indications to the necessity of a correct description of rheology in ice drift calculations are referred to the late 50s [*Ruzin*, 1959]. Subsequent to the simplest ice rheology models at present operating with viscous-plastic and cavitational rheolory are most widely used. The difference between these approaches will be considered below after the discussion of basic elements of thermodynamic models.

Modern-day dynamic (comprehensive) models of sea ice use as a component a thermodynamic unit, the essentials of which was developed within the framework of global climate models. The three-layer thermodynamic model of sea ice [*Semtner*, 1976], main principles of which are in common use at present, is a certain generalization in term of construction of one-dimensional numerical models. In this work it is shown that the reduction of layers number to minimum in the suggested scheme does

not influence substantially the results and it is rather beneficial in view of the consumption of computational resources compared to a multi-layer model [*Maykut and Untersteine*, 1971].

The balance equation for heat fluxes on ice-snow upper and lower surfaces are used for ice melting/accretion calculations (the upper layer in the three-layer scheme represents the snow phase). Heat flux in the snow-ice interface is continuous while crossing the boundary.

The heat balance equation on the upper ice surface (or snow if exists) is written in the following way:

$$F_A = F_l + F_t + F_L + (1-\alpha)F_r + \sigma T_s^4 , \qquad \text{(E.4)}$$

where F_A is the net heat flux on the upper ice surface;
F_l is the heat flux due to evaporation from the surface (latent heat flux);
F_t is the sensible heat flux;
F_L is the downward long-wave radiation flux;
F_r is the downward short-wave (direct and scattered) solar radiation;
α is the surface albedo;
σ is Stefan-Boltzmann constant;
T_s is the surface temperature. All the fluxes are assumed positive if they are directed upward.

If snow is available on the ice surface, F_A is compared with the heat flux inside the snow F_s defined by its heat conduction:

$$F_s = k_s \frac{T_0 - T_s}{h_s / 2} , \qquad \text{(E.5)}$$

where k_s is the thermal diffusivity of snow;
T_0 is the temperature in the middle of the snow layer;
h_s is the snow-layer thickness.

From the surface heat balance condition, $F_A = F_s$, after substitution into it expressions for F_A and F_s one derives the relationship for the underlying surface temperature T_s. If T_s determined in such a way reaches the freezing point, then the excess heat F_A - F_s is spent for snow melting. Snow depth changes Δh over a time step are given by the relationship:

$$\Delta h_s = \Delta t (F_A - F_s) / q_s , \qquad \text{(E.6)}$$

where q_s is the specific heat of snow melting.

In the absence of snow on the ice surface similar equations are solved with substitution of thermodynamic ice parameters for snow parameters.

In the work [*Semter*, 1976], in addition to the above mentioned parameters, processes of ice thickness variation due to bottom melting/accretion were considered; snow thickness increase at falling the precipitation solid fraction; the effect of heat accumulation and waste in salt pockets. Basic physical principles and the numerical scheme suggested in [*Semtner*, 1976] are used in the majority of thermodynamical sea ice models.

An example of more complete model involving, along with thermodynamics, the description of ice cover dynamics is the model of [*Flato and Hibler*, 1992] based on the approach suggested in the 60s by *Nikiforov et at*. [1967]. The dynamic model unit is developed within the approximation of cavitating

fluid, according to which ice resists to the compression (convergence), but it can be freely distributed over the basin if there are areas free of ice. Chronologically, this model appeared later than more sophisticated dynamic model of *Hibler* [1979], which was commonly used and in many respects defines the development of sea ice models up till now.

In the model [*Hibler*, 1979] the mechanical behaviour of the ice cover is described within the approximation of viscous-plastic solid medium, i.e. along with the action of tangential (viscous) stresses arising in the course of compact ice motion, plastic deformations at normal stresses leading to ice cover hummocking are taken into account. The equation of ice dynamics in the vector form is written as follows:

$$m D\bar{u}/Dt = -mf\vec{k}\times\bar{u} + \vec{\tau}_a + \vec{\tau}_w - mg\vec{\nabla}H + \vec{F}\ , \tag{E.7}$$

where $D/Dt = \partial/\partial t + \bar{u}\cdot\vec{\nabla}$ is the total time derivative;

$\vec{k}$ is the normal to the surface vector;

$\bar{u}$ is the vector of ice motion velocity;

f is the Coriolis parameter;

m is the ice mass per unit area;

$\vec{\tau}_a$, $\vec{\tau}_w$ are the vectors of wind and water stress;

H is the dynamic height of the sea surface;

g is the gravity acceleration;

$\vec{F}$ is the force of internal stress.

For the stresses induced by wind and water friction the following expressions are used:

$$\vec{\tau}_a = \rho_a C_a \left|\bar{U}_a\right| (\bar{U}_a \cos\phi + \vec{k}\times\bar{U}_a \sin\phi)\ , \tag{E.8}$$

$$\vec{\tau}_w = \rho_w C_w \left|\bar{U}_w - \bar{u}\right| ((\bar{U}_w - \bar{u})\cos\theta + \vec{k}\times(\bar{U}_w - \bar{u})\sin\theta) \tag{E.9}$$

where $\bar{U}_a$ is the wind speed vector;

$\bar{U}_w$ is the sea current velocity vector;

C, C_w are the friction coefficients for the atmosphere and water respectively;

ρ_α, ρ_w are the density of air and water respectively;

ϕ, θ are the angular rotation of wind and sea current stresses.

Components of internal friction forces $F_i = \partial\sigma_{ij}/\partial x_i$ are expressed through derivatives of tensor components of the medium stress σ_{ij}. For viscous-plastic medium the stress tensor components are expressed through components of deformation rate tensor ε_{ij} and pressure P in the following way:

$$\sigma_{ij} = 2\eta(\overset{*}{\varepsilon}_{ij}, P)\overset{*}{\varepsilon}_{ij} + [\xi(\overset{*}{\varepsilon}_{ij}, P) - \eta(\overset{*}{\varepsilon}_{ij}, P)]\overset{*}{\varepsilon}_{kk}\delta_{ij} - P\delta_{ij}/2\ , \tag{E.10}$$

$$\overset{*}{\varepsilon}_{ij} = \frac{1}{2}\left(\frac{\partial u_i}{\partial x_j} + \frac{\partial u_j}{\partial x_i}\right) \tag{E.11}$$

where δ_{ij} is the Kronecker symbol;

η, ξ are the bulk and shear of medium viscosity, x_i and x_j are the spatial co-ordinates.

In [*Hilber*, 1979] the following expressions were used for viscosity coefficients:

$$\xi = P / 2\nabla , \quad \eta = \xi / e^2 , \tag{E.12}$$

where $\nabla = [(\overset{*}{\varepsilon}{}^2_{11} + \overset{*}{\varepsilon}{}^2_{22})(1 + 1/e^2) + 4\overset{*}{\varepsilon}{}^2_{12}/e^2 + 2\overset{*}{\varepsilon}{}^2_{11}\overset{*}{\varepsilon}{}^2_{22}(1 - 1/e^2)]^{1/2}$;

e is the relation of axes of the main stress tensor.

The medium described by this rheological law experiences no internal stresses at pure divergence. The model developed within indicated approximations quite adequately simulates general features of sea ice drift and features of ice cover thickness associated with its dynamics. Among them - stationary region of maximum ice thickness near the northern coast of Greenland and Canadian Archipelago (Fig. E.27.c,d). Thermodynamic (one-dimensional) sea ice models cannot reproduce this structure even qualitatively.

At the same time, viscous-plastic models require large computer resources and the computational scheme can lead to computational instability [*Gray and Killworth,* 1995]. The appearance of cavitational models was, in part, an attempt to overcome these problems. The indicated difficulties are weakened partly by application of more effective numerical method [*Zhang and Hibler*, 1997].

In view of effective computational realization of sea ice model with the use of modern multi-processor computers it was suggested to employ more complicated rheological relationship [*Hunke and Dukowicz*, 1997].

Using similar notations the components of deformation rate tensor ε_{ij} and stress tensor σ_{ij} are connected by the expression:

$$\frac{1}{E}\frac{\partial \sigma_{ij}}{\partial t} + \frac{1}{2\eta}\sigma_{ij} + \frac{\eta - \xi}{4\eta\xi}\sigma_{kk}\delta_{ij} + \frac{P}{4\xi}\delta_{ij} = \overset{*}{\varepsilon}{}^2{}_{ij} , \tag{E.13}$$

where E is the Yuong module.

This rheological model is called elastic-viscous-plastic one. The model operates with two ice categories: thick and thin (up to 5 cm). In order to describe each category, different continuity equations are used: for ice compactness (specific area occupied by thick and thin ice), for mass (thickness) of thick and thin ice and for snow mass on the ice surface.

In other model [*Polyakov et al.,* 1997; *Polyakov*, 1999] more detailed description of horizontal inhomogenity of ice thickness field is achieved by introduction of six ice categories corresponding to gradations used in Russian monitoring network. In this model elastic-plastic rheology, which contrary to viscous-plastic approximation [*Hibler*, 1979] relates the stress in the ice cover not with the deformation rate tensor variation but with tensor itself.

In view of consideration of physical processes, more comprehensive model for the ice cover obviously is the model CSIM4 developed in US National Center of Atmospheric Research (NCAR). The model operates with five ice categories, elastic-viscous-plastic rheology, provides more detailed description of snow on the ice surface, improved model of surface albedo, salt pockets in ice, functional salinity profiles for each ice category etc. The detailed description of the model can be found in [*Hunke and Dukowicz,* 1997].

It might be well to point out that the comparison of results of this model with those obtained by a similar model with elastic-plastic rheology demonstrates [*Hunke and Zhang*, 1999] that in terms of reproducing long-term variability of the ice cover the results are actually identical but the first model is more effective from viewpoint of computations.

The considered models were employed both for problems of description of ice cover dynamics and as a constituent modules of climatic models.

E.5.2. *Brief description of the model for sea ice cover dynamics*

As a basis for calculations of required ice field characteristics the CSIM2 model was used. It is a constituent of the coupled model of the climate system, which is under development in NCAR within the framework of CCSM project [*Bruce et al.*, 2001]. In this model ice is affected by heat fluxes, various force fields and fresh water fluxes from the atmosphere and the ocean. In its turn ice affects atmospheric and oceanic processes by similar fluxes. Interaction processes of media in the NCAR model are described by a special interface module.

The model adaptation for computations of sea ice characteristics was limited to separation of CSIM2 module from the coupled climate model, to organize input of information about external boundary conditions (atmospheric forcing), tuning of model parameters and fulfillment of numerical experiments. Below we discuss basic information about thermodynamic and dynamic modules and results of the model application to simulations of the ice cover evolution in the Arctic.

The balance of vertical heat fluxes for snow-ice interface. Processes of vertical heat transfer are described by analogy with the model of *Semtner* [1976]. Two layers at total ice thickness exceeding 50 cm represent the total ice thickness. When ice thickness is between 25 cm and 50 cm, one ice layer is considered. If the ice thickness is less than 25 cm, zero-layer model is used. Snow on the ice surface is represented by one layer.
For the upper snow surface the balance equation for heat fluxes has the form:

$$S_1 + H_1 + L\uparrow_1 + k_s \frac{T_0 - T_s}{h_s / 2} = 0 \qquad \text{(E.14)}$$

where S_1 is the net solar radiation flux;

H_1 is the sum of fluxes of long-wave radiation, heat consumption for evaporation and turbulent heat exchange;

$L\uparrow_1$ is the upward long-wave radiation flux;

k_s is the heat conduction of snow;

h_s is the snow layer thickness;

T_s is the snow surface temperature;

T_0 is the temperature in the middle of snow layer.

The relationship for snow surface temperature (or ice in the absence of snow) is derived by substitution of $T_s = T_p + \Delta T$ (T_p is the surface temperature at the previous time step; ΔT is temperature increment per time step) in the heat balance Equation (E.14). At low ΔT expansion of Equation (E.14) into series upon ignoring the terms of higher orders yields:

$$S_1 + H_1 + L\uparrow_1 (T_p) + \Delta T\, 4\sigma (T_p)^3 + \Delta T \frac{\partial H_1}{\partial T_s} + k_s \frac{T_0 - T_p - \Delta T}{h_s / 2} = 0 \qquad \text{(E.15)}$$

From equation (E.15) the equation for ΔT can be derived. Similar algorithm can be applied to the case of the ice surface without snow.

Thermodynamic processes in polynyas. The formation of new ice at the water surface in polynyas and marginal regions is expressed by the relationship:

$$Q_H = Q_i \frac{d(A_i h_i)}{dt} \tag{E.16}$$

where Q_H is the net heat flux directed from the ocean to the atmosphere;
Q_i is the latent heat of ice freezing (melting);
A_i is the ice compactness;
h_i is the thickness of the forming ice.

It is assumed that the thickness of newly formed ice h_i^* is constant and equals 20 cm. In this case, for ice compactness increment from (E.16) we have:

$$\Delta A_i = Q_H \, \Delta t / (Q_i \, h_i^*) \tag{E.17}$$

After computation of new ice concentration the thickness of new and old ice in a cell is reduced to a single variable:

$$A_i' h_i' = A_i h_i + \Delta A_i \Delta h_i \tag{E.18}$$

where $A_{ii}' = A_i + \Delta A$, $\Delta h_i = h_i^*$.

The model assumes limitation for the maximum ice concentrations.

$$A_i' = \begin{cases} A_{\max} & h' \le 1\,\text{m} \\ 1-(1-A_{\max})\exp[-(h_i'-1)/\tau_1] & h' > 1\,\text{m} \end{cases} \tag{E.19}$$

The value A_{max} is assumed equal to 0.99 for the Northern Hemisphere and 0.96 for the Southern Hemisphere. The value τ_1 is selected equal to 3 m.

If the heat flux Q_H is directed from the atmosphere to the ocean, then a mechanism of lateral ice melting is acting, and the melting heat changes only the ice concentration. Processes of melting/accretion on the lower ice surface are not considered.

Evolution of snow cover on sea ice. The snow cover dynamics in the model involves processes of precipitation, evaporation, melting and conversion of snow into ice. Melting snow, snow from melting ice and snow entering the water in the absence of ice formation make a fresh water flow to the ocean. For the parameterization of the upper surface albedo the coefficient of snow distribution over the ice surface is introduced.

Ice cover dynamics and drift velocities. The dynamics of ice fields in cavitational approximation [*Flato and Hibler*, 1992] fits the medium behaviour, in which the final resistance is exerted to compression (convergence), but shear stress and resistance to divergence are absent. The equation of ice dynamics in spherical co-ordinates contains Coriolis forces, the stress induced by wind and sea currents, gravity forces arising due to sloping sea surface, and stress gradient due to ice compression:

$$\rho_i h_i f v_i + \tau_\lambda + C_w \cos\theta (u_w - u_i) - C_w \sin\theta (v_w - v_i) - \frac{\rho_i h_i g}{a\cos\phi}\frac{\partial \eta}{\partial \lambda} - \frac{1}{a\cos\phi}\frac{\partial p^*}{\partial \lambda} = 0 \,,$$

$$-\rho_i h_i f u_i + \tau_\phi + C_w \cos\theta(v_w - v_i) + C_w \sin\theta(u_w - u_i) - \frac{\rho_i h_i g}{a}\frac{\partial \eta}{\partial \phi} - \frac{1}{a}\frac{\partial p^*}{\partial \phi} = 0 \qquad \text{(E.20)}$$

where u_i, v_i are zonal and meridian components of ice velocity respectively;
ρ_i is the ice density;
h_i is the ice thickness;
f is the Coriolis parameter;
τ_γ, τ are the components of wins stress;
u_w, v_w are the components of current velocity;
C_w is the drag coefficient at the lower ice surface;
θ is the angular rotation of the vector of sea current effect;
η is the dynamic height of the ocean surface;
g is the acceleration of gravity;
α is the Earth's radius;
p^* is the pressure in ice.

Instead of original set of Equations (E.20) it is possible to write the transformed set:

$$-Du_i + Ev_i + X = \frac{1}{a\cos\phi}\frac{\partial p^*}{\partial \lambda},$$

$$-Dv_i - Eu_i + Y = \frac{1}{a}\frac{\partial p^*}{\partial \phi},$$

$$D = C_w \cos\theta, \qquad \text{(E.21)}$$

$$E = \rho_i h_i f + C_w \sin\theta,$$

$$X = C_w \cos\theta u_w - C_w \sin\theta v_w - \frac{\rho_i h_i g}{a\cos\phi}\frac{\partial \eta}{\partial \lambda} + \tau_\lambda$$

$$Y = C_w \cos\theta v_w + C_w \sin\theta u_w - \frac{\rho_i h_i g}{a}\frac{\partial \eta}{\partial \phi} + \tau_\phi,$$

in which expressions for D, E, X and Y do not depend on ice velocity.

The system of Equations (E.21) is solved by iteration with initial $p^* = 0$. For cells with $\nabla \cdot \bar{U}_i < 0$ correction term $\bar{U}_i'$ is introduced. It ensures non-divergence of the corrected velocity field,

$$\nabla \cdot (\bar{U}_i + \bar{U}_i') = 0 \qquad \text{(E.22)}$$

The conservation of the system of Equations (E.21) is possible in this case provided additional conditions for $\bar{U}_i'$ are fulfilled:

$$-D\bar{U}_i' - E\bar{k} \times \bar{U}_i' = \nabla p' \qquad \text{(E.23)}$$

where p' is a certain correction pressure in a cell resisting convergent ice compression.

Velocity variations in a given cell may lead to the formation of convergent conditions in neighboring cells. In this case velocities and pressure in them are corrected to neutralize the convergence. This algorithm is applied in iterative way for the entire computation domain till conditions:

$$\max\left(\left|\bar{U}_i^n\right| - \left|\bar{U}_i^{n-1}\right|\right) < 0.002 \text{ m/s} \qquad \text{(E.24)}$$

are fulfilled.

The mechanism of correction pressure may be used until the pressure in a cell reaches its maximum,

$$P_{\max} = P^* h_i \exp[-20(1-A_i)] \tag{E.25}$$

In zones with constant convergence at correcting pressure exceeding the maximum excess convergence is distributed over cells without convergence.

Advection. The advection transport in the model affects all mass and thermodynamic parameters connected with sea ice. Upstream advection scheme is used:

$$\frac{\partial f}{\partial t} = -\nabla \cdot (f\vec{U}_i) \approx (u_l f_l \Delta y - u_r f_r \Delta y + v_b f_b \Delta x_b - v_t f_t \Delta x_t)/\Delta A \tag{E.26}$$

where indices *l, r, b, t* imply that values belong to the left, right, lower (southern) and upper boundaries of a cell respectively. For the pole cell advection is specified as a sum of fluxes from cells neighboring all southern boundaries of the pole cell. In the model, instead of Equation (E.26), its analog in terms of ice velocity divergence is used:

$$\frac{\partial f}{\partial t} \approx -2\nabla \cdot \vec{U}_i \frac{f_l + f_r + f_b + f_t}{4} + \frac{\partial v_i}{\partial y}\frac{(f_l + f_r)}{2} + \frac{\partial u_i}{\partial x}\frac{(f_b + f_t)}{2} + \left\{\frac{u_l + u_r}{2}(f_l - f_r)\Delta y + \frac{v_b \Delta x_b + v_t \Delta x_t}{2}(f_b - f_t)\right\}/\Delta A. \tag{E.27}$$

The correction for excess convergence in cells with stable convergence is made in the following way:

$$f_n'' = f' \frac{(\bar{f}A - \bar{f}_m' A_m)}{\bar{f}_n' A_n} \tag{E.28}$$

where f_n'' are the new values of corrected values for points with positive divergence;

f_n' are the previous values of the corrected variables for points with positive divergence;

$\bar{f}_n'$ is the mean value for the hemisphere;

A are the cell areas, indices m and n are referred to cells with negative and positive divergence respectively.

Consideration of oceanic processes. Among essential parameters defining the ice cover evolution is the heat flux at the ice-water interface. Though mean flux value is only several W/m^2 its long-term effects can result in essential redistribution of the ice cover. In combined models this heat flux is computed in the ocean model and it is delivered to the ice model as an external parameter.

In our case when the ice model is not directly connected with the ocean one the heat flux at the lower ice boundary should be determined with the use of additional conditions. One of reasonable approaches is the application of temperature of the upper mixed layer (as a rule coinciding with the ocean surface temperature) for computation of its enthalpy and heat flux using the difference in temperatures between water and ice. The latter is assumed to be equal to freezing point (typical value under Arctic conditions is –1.8^{o}C).

Simpler but rather crude way of the parameterization of heat exchange processes at the water-ice interface is the prescription of constant heat flux. Obviously it is acceptable only in short-term calculations.

E.5.3. *Computation procedure*

Prior to main calculations of ice characteristic evolution over a year time interval there was a stage of preparation of appropriate computation environment. It involves the configuration of the model domain, tuning of model parameters, preparation of atmosphere forcing fields specifying external (boundary) conditions for the model.

The ice cover dynamics model domain is represented by a grid superimposed on the sphere with grid points arranged according to B-grid of Arakawa's Classification. On the entire sphere the grid dimension is 150×110. Along the longitude the grid is uniform with spatial resolution 2.4°. Along the latitude the gridsize is 1.2° in latitude belts from the pole to 60°S and 60° N. In low latitudes the gridsize is larger. Time step is 20 min.

In a general case input data for the ice cover model integrations involve the following fields:

- wind stress at the upper ice surface and ocean current stress at its lower surface;
- solar radiation flux at the upper ice surface minus the reflected part;
- sum of fluxes of downward long-wave radiation, heat consumption for evaporation and turbulent heat exchange at the upper ice surface;
- derivative of the sum of fluxes including downward long-wave radiation, heat consumption for evaporation and turbulent heat exchange at the upper ice surface by the temperature of this surface $\partial H_l / \partial H_T$;
- heat flux at the ice-water interface determined by potential enthalpy of the upper ocean surface;
- fresh water flux at the ice/snow interface;
- water surface slope.

To estimate these fields, a dataset of the reanalysis of meteorological fields [*Kalnay et al.,* 1996] was used. Mean monthly fields of relevant characteristics were used as initial ones. The reanalysis data are presented on a uniform geographical grid with dimension 144×72 with gridsize 2.5°×2.5°. With the use of bilinear interpolation these data were put on the knots of computation grid. When integrating the ice model atmospheric forcing was updated daily and the forcing fields were determined through the interpolation of mean monthly values. Derivative $\partial H_l / \partial T_s$, which is not incorporated to this dataset, was determined from expressions for turbulent heat exchange and heat consumption for evaporation in the following way:

$$\frac{\partial H_1}{\partial T_s} = -\left|\bar{U}_a\right|(c_a k_t + L k_l k_q k_{sat} / P \exp(a T_a /(T_a + b)) a b /(T_a + b)^2 \qquad \text{(E.29)}$$

where c_α is the specific heat of air;
L is the specific heat of evaporation;
T_α is the air temperature at the reference height (usually 2 m);
$\bar{U}_a$ is the wind speed at the reference height (usually 10 m);
P is the atmospheric pressure;
k_{sat}, a, b are the coefficients in Magnus formula for saturated humidity;
k_t, k_l are the coefficients of heat- and moisture exchange in the near water air layer.

The required initial fields of ice characteristics were specified in two ways. In the first case constant thickness and compactness of ice were used as initial data, in the second case we employed fields

determined from numerical experiments with a coupled climate model used under CCSM project [*Bruce et al.,* 2001].

After preliminary model testing and tuning the required annual data set of sea ice characteristics has been calculated. Prior to these calculations integration for five years to spin-up the model and its adjustment to atmospheric forcing fields repeating in a cycling way from year to year were performed. Computations were made in local (thermodynamic) approach – neglecting dynamic processes, i.e. with zero ice drift velocity.

E.5.4. *Preliminary results*

In the course of integration of the sea ice model mean monthly fields of the following characteristics of sea ice were calculated and stored in the set of files for one year:

- ice thickness,
- ice compactness,
- ice/snow surface temperature,
- snow thickness on the ice,
- snow melting rate,
- ice melting rate at the upper boundary,
- ice melting rates at the lower and lateral boundaries.

Figure E.27 demonstrates the simulated distribution of sea ice thickness and compactness for December and August. A large-scale structure of simulated fields is mainly consistent with distributions obtained from observations. Seasonal variations of ice cover extension are accompanied by typical reduction of ice compactness. By summer the region of compact ice (9-10 balls) decreases by 3-4 times and it is located near the northern coast of Greenland and Canadian Archipelago (Figs. E.27.a,b). Similar area is occupied by ice with compactness 7-9 balls and much smaller regions are occupied by ice of less compactness. The formation of tongues protruded in the meridianal direction to the Greenland Sea and the Labrador Sea and the Sea of Okhotsk characterize the distribution of winter ice. This is one of prominent features of the ice cover which have no analogy in the Antarctic.

The basic large-scale structure is well enough reproduced in fields of ice thickness in winter and summer – the region of the most powerful perennial ice (Figs. E.27 c,d).

The notable discrepancy between model and climatic fields is observed in the Barentz Sea where the ice cover is overestimated especially during winter period (Fig. E.27.a). As it was mentioned above heat transport by ocean currents impedes the formation of ice. These effects are not described by a given model, and for their adequate consideration it is necessary to employ a coupled ocean-sea ice model.

Great seasonal variations of sea ice area essentially affect processes of contaminants distribution. In winter the ice cover over the major part of the Arctic screens out the direct exchange of contaminants being in different phases between the atmosphere and the ocean. During warm season the contact area increases approximately 2 times. From the onset of sea ice intensive-melting contaminants trapped by ice enter the ocean. For a correct account of these processes information about phase transfer of sea ice should be available. For this reason fields on intensive ice and snow melting are referred to essential calculation parameters.

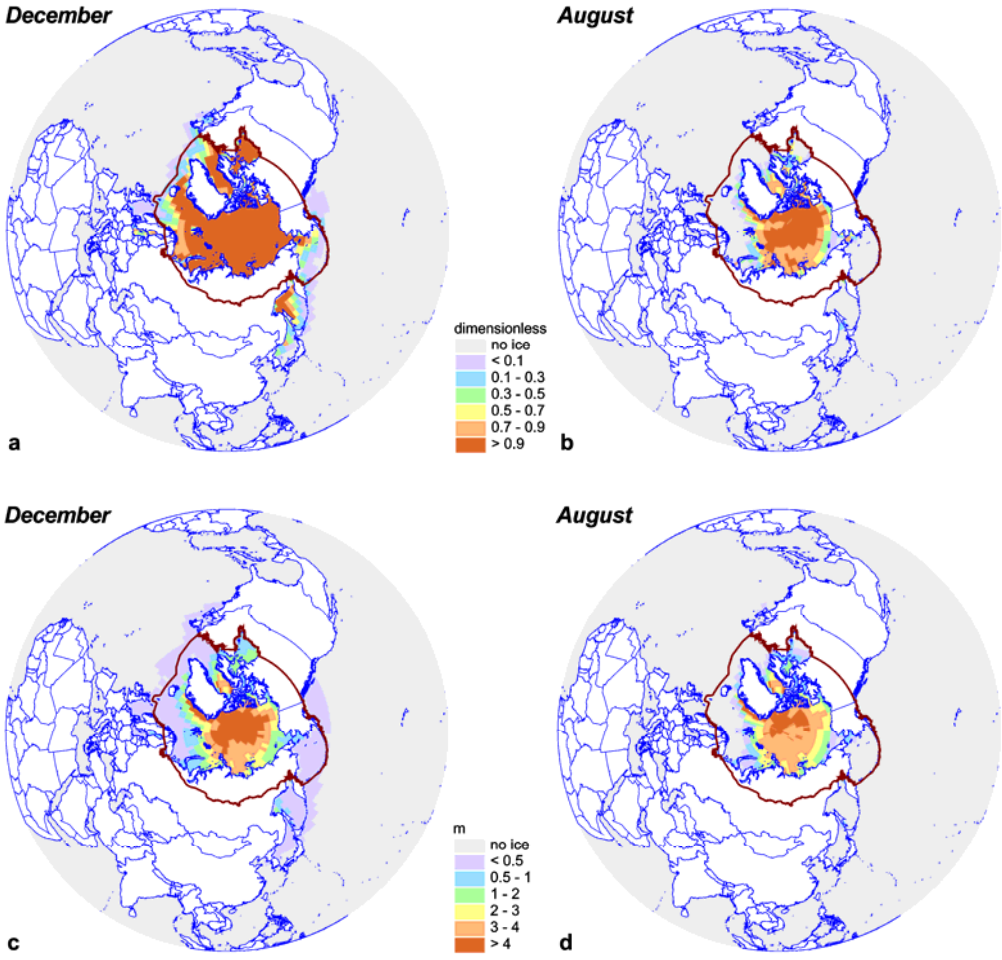

Figure E.27. *Simulated distribution of ice compactness (a) and (b) and thickness (c) and (d) in December and August*

Figure E.28 shows simulated fields of ice melting rate at the upper and lower boundaries for winter and summer seasons. Essential melting of the ice cover takes place on its surface mainly due to incoming short-wave radiation beginning from April. Melting stage is sufficiently shorter than the processes of ice accretion extended over a year. This asymmetry results in a kind of a “volley” discharge (June-July) of melted water to the ocean with all dissolved contaminants. Ice thickness variation at its lower boundary is characterized by much lower values (in Fig. E.28.b another color scale is used). However, the operation with these values should be very careful because the effect of oceanic processes on ice evolution is rather schematic in this model. More reliable data can be obtained with the use of a coupled ocean–sea ice model.

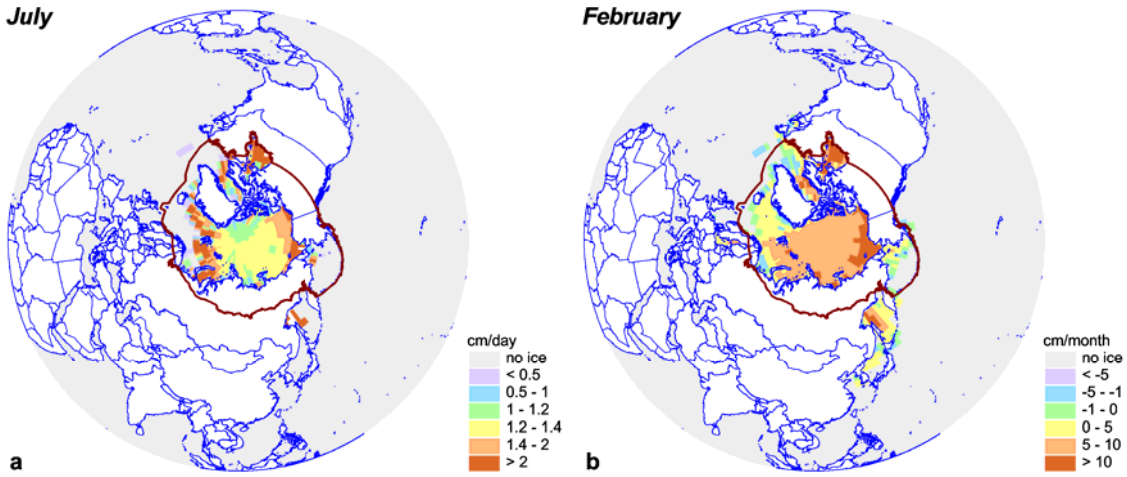

Figure E.28. *Field of ice cover melting rates at upper boundary (a) in July and at the lower boundary (b) in February*

Similar processes are related to the snow cover evolution on the ice surface (Fig. E.29.a). This cover also melts fast compared to the period of its accumulation. Although the rate of snow melting (Fig. E.29.b) is comparable with the ice melting rate (Fig. D.28.a) this source is less important for the transport of water and contaminants from the atmosphere to the ocean for the reason of rather thin snow cover (Fig. E.29.a). The latter is connected with the establishment of arctic anticyclone and week precipitation. More intensive precipitation falls along the periphery of the anticyclone over Arctic sea basins (Fig. E.29.a).

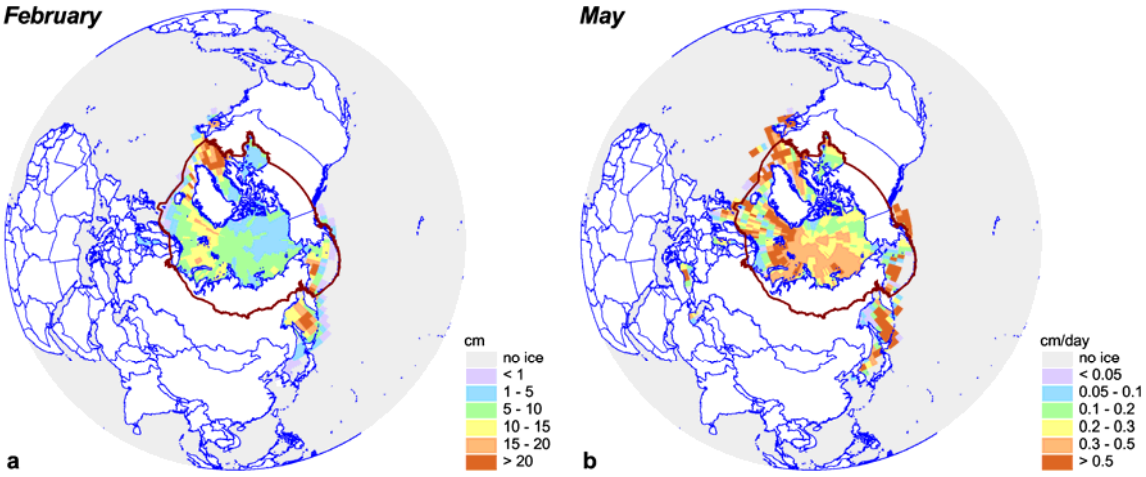

Figure E.29. *Snow cover thickness in February (a) and snow melting rate in May (b)*

Considering the obtained results as a whole it should be mentioned that model calculations make it possible to estimate characteristics of sea ice representing basic large-scale features of its evolution. In particular these data are applicable to the evaluation of impact on contaminants dispersion of such processes as ice screening impeding the exchange between the ocean and the atmosphere and comparatively long accumulation of contaminants in ice and their “rapid” discharge to the ocean during melting. To obtain more detailed and more accurate data on ice cover evolution comprehensive models of sea ice should be applied.

E.5.5. *Further activity*

The obtained results are of a preliminary character and are intended for acquisition of qualitative estimates of the impact of the Arctic ice cover on contaminants distribution processes. To investigate in detail the sea ice behaviour it is supposed both further development of the model and application of more detailed characteristics of atmospheric forcing.

In order to improve the quality of calculated fields it is necessary to use a coupled model for ocean-sea ice since processes occurring in both media are closely connected. As follows from some investigations a number of important characteristics of ice cover evolution cannot be reproduced without adequate account of the influence of oceanic currents and heat redistribution processes associated with them.

For a correct description of the distribution of ice thickness and its variability, it is necessary to consider ice dynamics. Recent results show that the observed features are reproduced best of all by models with viscous-plastic rheology or its close variations. Therefore in further research connected with calculations of the Arctic ice evolution models of this type should be used.

A correct representation of the ice cover behaviour is closely connected with adequate specification of atmospheric forcing. In its importance, along with seasonal scale, synoptic variability in the atmosphere is distinguished which results in a number of significant effects, which become apparent both in the ocean [*Resnyansky and Zelenko*, 1999] and in the behaviour of the ice cover. The role of short-term variations can be exemplified by the comparison [*Hanesiak and Barber,* 1999] of experimental results with hourly and daily mean forcing of one-dimensional thermodynamic ice model. An hourly forcing, keeping mean diurnal values, leads to earlier commencement of snow melting, and the duration of ice-free period increases by 21 days! It is related to non-linearity associated with the absorption of solar radiation and sensible and latent heat fluxes.

Therefore, to improve simulation results of ice cover evolution, it is necessary to pass on to atmospheric forcing fields taking into account synoptic variability (daily mean fields instead of monthly mean fields).

References

AMAP Report 2000: 3. PCB in the Russian Federation: Inventory and proposals for priority remedial actions. Arctic Monitoring and Assessment Programme (AMAP), Oslo, 2000, published by: Centre For International Project (CIP), Moscow, 2000.

Baldwin R.J., R.C.Glatts and K.L. Jr. Smith [1998] Particle matter fluxes into the benthic boundary layer at a long time-series station in the abyssal NE Pacific: composition and fluxes. Deep-Sea Research II, v. 45, 643-665.

Bruce P.B., C. Hunke, C.M. Bitz, B. Lipscomb and V. Schramm [2001] DRAFT description of the CCSM2 Sea Ice Model: CSIM4, (http://www.ccsm.ucar.edu/models/ice-csim4)

Dale T., F.Rey and B.R. Heimdal [1999] Seasonal development of phytoplankton at a high latitude oceanic site. Sarsia, v. 84, pp.419-435.

Dutkiewicz S., M.Follows, J.Marshall and W.Gregg Watson [2001] Interannual variability of phytoplankton abundances in North Atlantic. Deep-Sea Research II, v.48, pp.2323-2344.

Flato G.M. and W.D.Hibler [1992] Modeling pack ice as a cavitating fluid. *J.Phys.Oceanogr.*, v.22, pp.626-651.

Garcon Veronique C., Andreas Oschlies, Scott C. Doney, Dennis McGillicuddy, Joanna Waniek [2001] The role of mesoscale variability on plankton dynamics in the North Atlantic.

Gray J.M.N.T. and P.D. Killworth P.D. [1995] Stability of the viscous-plastic sea ice rheology. *J. Phys. Oceanogr.*, v. 25, No 5, pp. 971-978.

Hanesiak J.M. and D.G. Barber [1999] Role of diurnal processes in the seasonal evolution of sea ice and its snow cover. *J. Geophys. Res.*, v. 104, No C6, pp. 13593-13603.

Hibler III W. D. [1979] A dynamic thermodynamic sea ice model. *J. Phys. Oceanogr.*, v.9, No.4, pp. 815-846.

Hunke E.C. and J.K.Dukowicz [1997] An elastic-viscous-plastic model for sea ice dynamics. *J. Phys. Oceanogr.*, v. 27, pp. 1849-1867.

Hunke E.C. and Y. Zhang [1999] A comparison of sea ice dynamics models at high resolution. *Mon. Wea. Rev*., v. 127, pp. 396-408.

Jackson George A., and B. Burd Adrian [2002] A model for distribition of particle flux in the mid-water column controlled by subsurface biotic interactions. Deep Sea Research Part II: Topical Studies in Oceanography, v. 49, pp.193-217

Kalnay et al., 1996 Kalnay E.,Kanamitsu M.,Kistle R.,Collins W., Deaven D., Gandin L., Iredell M., Saha S., White G., Woollen J., Zhu Y., Leetmaa A., Reynolds R., Chelliah M., Ebisuzaki W., Higgins W., Janowiak J., Mo K.C., Ropelewski C., Wang J., Roy Jenne, and Dennis Joseph The NCEP/NCAR 40-Year Reanalysis Project // Bulletin of the American Meteorological Society, 1996, vol. 77, No. 3, p. 437-471.

Macdonald R.W., Barrie L.A., Bidleman T.F., Diamond M.L., Gregor D.J., Semkin R.G., Strachan W.M., Li Y.F., Wania F., Alaee M., Alexeeva L.V., Backus S.M., Bailey R., Bewers J.M., Gobel C., Halsall C.J., Harner T., Hoff J.T., Jantunen L.M.M., Lockhart W.L., Mackay D., Muir D.C.G., Pudykiewicz J., Reimer K.J., Smith J.N., Stern G.A., Schroeder W.H., Wagemann R., Yunker M.B. [2000] Contaminants in the Canadian Arctic: 5 years of progress in understanding sources, occurrence and pathways. *The Science of the Total Environment*, V. 254, pp. 93-234.

Maykut G.A.and N.Untersteine [1971] Some results from a time-dependent thermodynamic model of sea ice, *J.Geophys.Res.,* v.76, p.1550-1575.

Monin A.S. (ed.) [1997] Oceanic biology. M., “Nauka”.

Nikiforov Ye.G., Z.M. Gudkovich, Yu.N. Yefimov and M.A. Romanov [1967] Principles of a method for calculating the ice redistribution under the influence of the wind during the navigation period in the Arctic seas. Tr. Arkt., Antarkt. Int., v. 257, pp. 5-25.

Pacyna J.M. et al. [1999] Final report for Project POPCYCLING-Baltic. EU DGXII, Environment and Climate Program ENV4-CT96-0214. Available on CD-rom including technical report, the emission and environmental databases as well as the POPCYCLING-Baltic model. NILU, P.O. Box 100, N-2027 Kjeller, Norway.

Pfirman S.L., H.Eicken, D.Bauch and W.F. Weeks [1995] The potential transport of pollutants by Arctic sea ice. *Science of the Total Environment* (NLD), v.159, pp.129-146.

Polyakov I.V. [1999] Modeling the Arctic ocean seasonal variability, *Okeanologiya*, v.39, No.4, pp.493-503, (*in Russian*).

Polyakov I.V., Kulakov I.Yu., Kolesov S.A. et al. [1997]. Dynamic-thermodynamic model of the ocean covered with ice: description and experiments. Izvestia of the Russian Academy of Sciences. Physics of the atmosphere and Ocean, v.37, No.4, (*in Russian*).

Resnyansky Yu.D. and A.A. Zelenko [1999] Effects of synoptic variations of atmospheric impacts in the model of ocean general circulation: direct and indirect manifectation. *Meteorology and Hydrology*, No.9, pp.66-71, (*in Russian*).

Resnyansky Yu.D. and A.A.Zelenko [1999] Effects of synoptic variations of atmospheric forcing in an ocean general circulation model: direct and indirect manifestation. Meteorology and Hydrology, No.9 pp.66-77.

Ruzin M.I. [1959] The wind drift of ice in a heterogeneous pressure field. Tr. Arkt., Antarkt. Int., v. 226, pp. 123-135.

Schulz-Bull D.E., G.Petrick, R. Bruhn and J.C. Duinker [1998] Chlorobiphenyls (PCB) and PAHs in water masses of the northern North Atlantic; *J.Marine Chemistry* (NLD); v.61; No.1-2; pp.101-114.

Semtner A.J. [1976] A model for the thermodynamic growth of sea ice in numerical investigations of climate. J. Phys. Oceanogr., v. 6, pp. 379-389.

Tusseau M.-H., C.Lancelot, J.-M.Martin and B.Tassin [1997] 1-D coupled physical-biological model of the northwestern Mediterranean Sea. Deep-Sea Research II, v. 44, No 3-4, pp.851-880.

Zhang J. and W.D. Hibler III [1997] On an efficient numerical method for modeling sea ice dynamics. *J. Geophys. Res.,* v. 102**,** No C4, pp. 8691-8702.